ISSN 0965-5425, Computational Mathematics and Mathematical Physics, 2015, Vol. 55, No. 4, pp. 628–637. © Pleiades Publishing, Ltd., 2015.
Original Russian Text © A.M. Gumerov, E.G. Ekomasov, R.R. Murtazin, V.N. Nazarov, 2015, published in Zhurnal Vychislitel'noi Matematiki i Matematicheskoi Fiziki, 2015, Vol. 55, No. 4, pp. 631–640.

Transformation of Sine-Gordon Solitons in Models with Variable Coefficients and Damping

A. M. Gumerov[a], E. G. Ekomasov[a], R. R. Murtazin[a], and V. N. Nazarov[a, b]

[a] *Bashkir State University, ul. Zaki Validi 32, Ufa, 450076 Bashkortostan, Russia*

[b] *Institute of Physics of Molecules and Crystals, Ufa Research Center, Russian Academy of Sciences, pr. Octyabrya 151, Ufa, 450075 Russia*

e-mail: bgu@bk.ru, ekomasoveg@gmail.com

Received June 16, 2014; in final form, October 6, 2014

Abstract—The dynamics of sine-Gordon solitons in the presence of an external force, damping, and a spatially modulated periodic potential is studied. Numerical methods are used to show the possibility of generating localized nonlinear waves of the soliton and breather types. Their evolution is investigated, and the dependences of the amplitude and the oscillation frequency on the parameters of the system are found.

DOI: 10.1134/S096554251504003X

Keywords: kink, breather, soliton, sine-Gordon equation, spatially modulated periodic potential.

INTRODUCTION

In recent years, the dynamics of solitons has attracted increasing interest [1], which is motivated by their numerous physical applications [2–4]. For example, in solid state physics, sine-Gordon solitons describe domain boundaries in magnets, dislocations in crystals, fluxons in Josephson junctions, etc.

Aimed at the construction of models describing actual physical processes, a task of interest is to study the influence exerted by perturbations of various shapes on the dynamics and structure of sine-Gordon solitons. For example, much research has been focused on the influence of a coordinate- and time-dependent external force and a spatial modulation of the periodic potential (SMPP) (see, e.g., [2–9]). The effect of small perturbations on sine-Gordon solutions can be examined with the help of well-developed perturbation theory for solitons [3–6, 9–10], while the influence of large perturbations can generally be investigated only by applying numerical methods (see [6, 11–14]).

Consider the following modified sine-Gordon equation, which appears, for example, in describing the dynamics of domain boundaries in multilayered ferromagnets [15]:

$$\frac{\partial}{\partial x}\left(A(x)\frac{\partial\theta}{\partial x}\right)-\frac{\partial^2\theta}{\partial t^2}-\frac{1}{2}K(x)\sin 2\theta = h\sin\theta+\alpha\frac{\partial\theta}{\partial t}. \tag{1}$$

Here, $A(x)$ and $K(x)$ are functions characterizing the spatial modulation of the parameters, h is an external force parameter, and α is a damping constant. In the case of arbitrarily varying K and A, Eq. (1) can be solved only with the help of numerical methods.

When $A(x) = K(x) = 1$ and $h = \alpha = 0$, Eq. (1) passes into the well-known sine-Gordon equation, which has the kink solution

$$\theta(x,t) = 2\arctan\left(\exp\left[\Delta(v_0)(x-v_0t)\right]\right), \tag{2}$$

where $\Delta(v) = 1/\sqrt{1-v^2}$ and v_0 is a continuous parameter ($0 < v_0 < 1$) determining the velocity of the kink. The sine-Gordon equation also has spatially localized solutions, such as a breather at rest,

$$\theta_{\text{breather}}(x,t,\omega) = 2\arctan\left(\frac{\sqrt{1-\omega^2}\sin\omega t}{\omega\cosh\left(\sqrt{1-\omega^2}\,(x-x_0)\right)}\right), \tag{3}$$

where ω is the frequency of the breather and x_0 is the coordinate of its center, and a soliton solution of the form

$$\theta_{\text{kink-antikink}}(x,t,\omega) = 2\arctan\left(\frac{1}{v_0}\frac{\sinh[\Delta(v_0)t]}{\omega\cosh(\Delta(v_0)(x-x_0))}\right). \quad (4)$$

The dynamics of sine-Gordon solitons in the case of $A(x) = 1$, $h = \alpha = 0$, and a steplike "point SMPP" of the form $K(x) = 1 - \varepsilon\delta(x)$, where $\delta(x)$ is the Dirac delta function and $0 < \varepsilon < 1$, was investigated in detail by applying analytical and numerical methods (see [3–6, 16]). It was shown that, in the case of an "undeformable kink," the SMPP acts as a potential. With a suitable sign of ε ($\varepsilon > 0$), it acts on a kink as an attracting potential, so sine-Gordon solitons can be localized and radiate. The possibility of exciting a localized mode in kink scattering, which has a large effect on the kink dynamics, was also taken into account. It was shown numerically and analytically in [17–19] that the resonance interaction of a kink with an excited localized mode is possible in the case of an extended SMPP. The structure and properties of localized nonlinear waves excited by one- and two-dimensional SMPPs were analyzed numerically in [20, 21]. In the case of two identical SMPPs [22–24], it was shown that strong combined effects and four-kink states can appear in the system. The transmission, capture, and reflection of a pair of kinks in the presence of SMPP were also studied (see, for example, [25, 26]).

In the case of $A(x)$ and $K(x)$, perturbation theory and numerical methods were used to study the dynamics of a kink in the presence of a steplike point SMPP with a Dirac delta function and an extended SMPP of rectangular shape [15, 27, 28]. In this paper, the dynamics of a kink is investigated with allowance for the possibility of exciting large-amplitude nonlinear localized waves by the SMPP region in the presence of an external field and damping.

1. NUMERICAL SOLUTION METHOD

Consider a kink of form (2) moving at a constant velocity v_0 through the SMPP region. The spatial modulation of the parameters $A(x)$ and $K(x)$ in Eq. (1) is modeled using a Gaussian-type function:

$$K(x) = 1 + \Delta K \cdot \cosh^{-2}(4(x - x_0)/W), \quad (5a)$$

$$A(x) = 1 + \Delta A \cdot \cosh^{-2}(4(x - x_0)/W), \quad (5b)$$

where W is a parameter characterizing the SMPP width, x_0 is the position of its center, $\Delta K = K - 1$, K is the parameter value at the point x_0, $\Delta A = A - 1$, and A is the parameter value at the point x_0. The boundary conditions are specified as

$$\theta(-\infty, t) = 0, \quad \theta(+\infty, t) = \pi. \quad (6)$$

Exact solutions of Eq. (1) can be obtained only in special cases, and analytical methods (e.g., perturbation theory) work, as a rule, only in bounded ranges of system parameters. Currently, a variety of numerical methods are available for solving such equations. For example, a compact finite-difference scheme and a DIRKN method are used in [29]. The compactness of the scheme lies in that its recurrence formula for new time level computation consists of at most nine stencil points, including the central one, near which the derivatives are approximated. By a DIRKN method, we mean the class of diagonal implicit Runge–Kutta–Nyström methods (more detail about these methods can be found, e.g., in [30]). In [31] the sine-Gordon equation is solved numerically using collocations and radial basis functions. The method of lines is applied in [32]. The spectral and pseudospectral Fourier methods are used to solve sine-Gordon-type equations in [26, 33–35]. A meshless scheme relying on multiquadratic quasi-interpolation is presented in [36]. This method does not require solving large-scale systems of linear algebraic equations. Various predictor–corrector schemes are used in [37, 38]. A method based on reproducing kernels in Hilbert spaces is applied in [39].

In this paper, Eq. (1) is solved numerically using finite differences [40–42]. There are numerous versions of this method, which can be formally divided into explicit and implicit ones. We use a three-level explicit scheme with derivatives approximated on a five-point cross-type stencil, which was used earlier

for simpler sine-Gordon equations (see, e.g., [22, 23]). Approximating the original differential equation on this stencil yields the finite-difference equation

$$A(x_i)\frac{\theta_{i+1}^k - 2\theta_i^k + \theta_{i-1}^k}{\Delta x^2} + \frac{A(x_{i+1}) - A(x_{i-1})}{2\Delta x}\frac{\theta_{i+1}^k - \theta_{i-1}^k}{2\Delta x} - \frac{\theta_i^{k+1} - 2\theta_i^k + \theta_i^{k-1}}{\tau^2} - \frac{f(x_i)}{2}\sin 2\theta_i^k = h\sin\theta_i^k + \alpha\frac{\theta_i^{k+1} - \theta_i^{k-1}}{2\tau}. \tag{7}$$

Here, Δx is the spatial mesh size and τ is the time step. This numerical scheme is second-order accurate with respect to Δx and τ and conditionally stable: $(\tau/\Delta x) \le 1/2$.

In the case under study, the scheme consists of a single step, involves relatively few memory calls, and admits further optimization. Another convenience is that the scheme can be adapted with minor modifications to other versions of the one-dimensional equation (1) and to multidimensional sine-Gordon equations.

Boundary conditions (6) imply that particular values are specified on the grid boundaries. Numerical simulation based on iterative scheme (7) shows that waves reflect from the grid boundaries, thereby distorting the results when the simulation is long. Two approaches are usually used in such cases (see, e.g., [43, 44]). One of them makes use of an extended grid in coordinate and a process is studied in its central part until a certain critical time such that emitted waves have no time to reflect from the grid boundaries and return to the center. The idea of the other approach is that waves are absorbed near the domain boundary, which is preferable in terms of computational resources. Numerous types of absorbing conditions have been developed to date [45–48], including ones for second-order wave equations [49]. As a rule, the behavior of waves near the boundaries is described by special equations (for example, to implement Sommerfeld radiation conditions [45]). However, for Eq. (1), there is a simpler method. Specifically, the dissipative parameter α is defined as a piecewise constant function

$$\alpha = \begin{cases} 1, & x \le x_{\text{left}} + D_{\text{diss}}, \quad x \ge x_{\text{right}} - D_{\text{diss}}, \\ \alpha_0, & x_{\text{left}} + D_{\text{diss}} < x < x_{\text{right}} - D_{\text{diss}}, \end{cases} \tag{8}$$

where D_{diss} is the width of the absorption domain (as a rule, 3–5% of the width of the entire domain to be simulated) and α_0 is the value of the dissipative parameter in the main domain. As a result of using (8), all waves approaching the grid boundaries are nearly completely damped.

To estimate the error of the method, the values of $\theta(x_i, t_n)$ for fixed x_i and various t_k as computed from Eq. (1) are compared with its exact solution (2) (at $A(x) = K(x) = 1$ and $h = \alpha = 0$). The absolute error can be calculated using the formula

$$\Delta\theta = \left|\theta_{i,j}^n - 2\arctan[\exp((x_i - vt_k)/\Delta(v_0)]\right|, \tag{9}$$

and the normalized error is given by

$$\varepsilon = \Delta\theta/X_n, \tag{10}$$

where the normalizing value X_n is set equal to the upper limit of measurements; in our case, $X_n = \pi$. The numerical simulation has shown that errors are accumulated over time, but the error growth rate is rather slow. Even for the large parameter value $t = 500$, the error is $\varepsilon \approx 0.0125\%$.

2. INTERACTION OF A KINK WITH AN IMPURITY

First, we consider a kink that keeps moving without damping. As is known, SMPP can create a potential well or a potential barrier for the moving kink, and its energy is reduced or increased because of the interaction with the impurity. Figure 1 presents the numerically computed minimum velocity $v_{\min}(\Delta A, \Delta K)$ at which the kink passes through the SMPP region. The results show that the effect of ΔK on $\upsilon_{\min}$ is noticeably larger than that of ΔA (see curves (*1*)–(*4*) in Fig. 1b). The curves in Fig. 1b for $\Delta > 0$ and $\Delta < 0$, where $\Delta = \Delta A + \Delta K$, are not symmetric. This can be explained by the fact that the velocity of the kink and, hence, its kinetic energy, increase when it overcomes the potential well at the initial time. Thus, the kink escapes the SMPP region at a higher velocity than the initial one, thus reducing $v_{\min}$. In the case of a potential barrier, on the contrary, as the kink approaches the SMPP region, its velocity first decreases, thus increasing $v_{\min}$. For $\Delta A + \Delta K < 0$, in contrast to the analytical case, when the kink velocity is lower than $v_{\min}$, the kink is localized on the potential well (Fig. 2). The kink structure varies with time. In addition to exciting

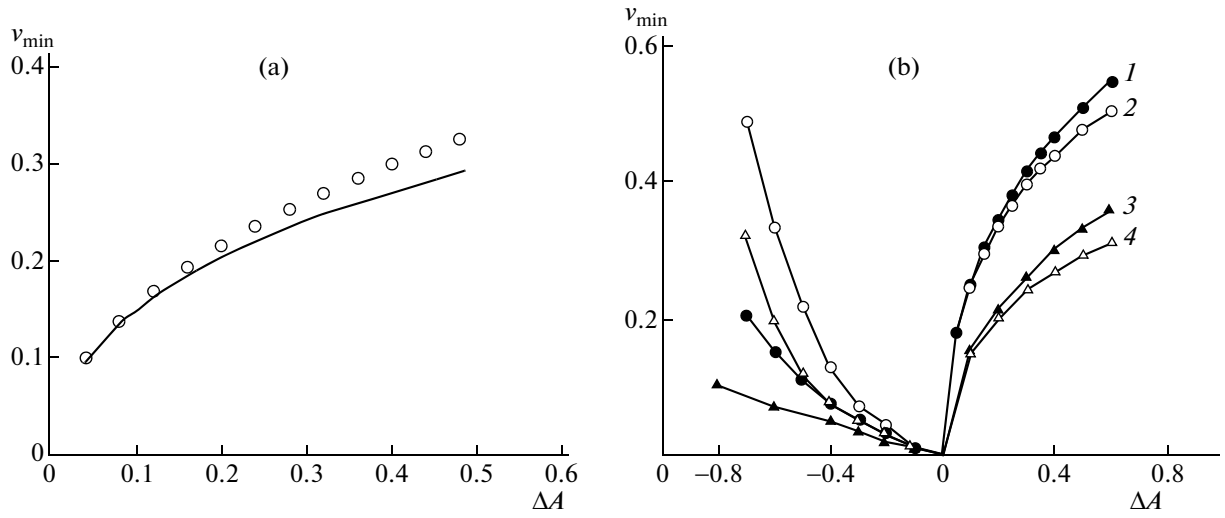

Fig. 1. Minimum kink velocity v_{min} as a function of (a) ΔA for $\Delta K = 0$, $W = 1$, $h = 0$, and $\alpha = 0$ (circles show the solution of system (14), (15), while the solid curve depicts the numerical solution of Eq. (1)) and as a function of (b) $\Delta = \Delta K + \Delta A$ for (*1*) $\Delta A = 0$, $W = 4$; (*2*) $\Delta K = 0$, $W = 4$; (*3*) $\Delta A = 0$, $W = 1$; and (*4*) $\Delta K = 0$, $W = 1$.

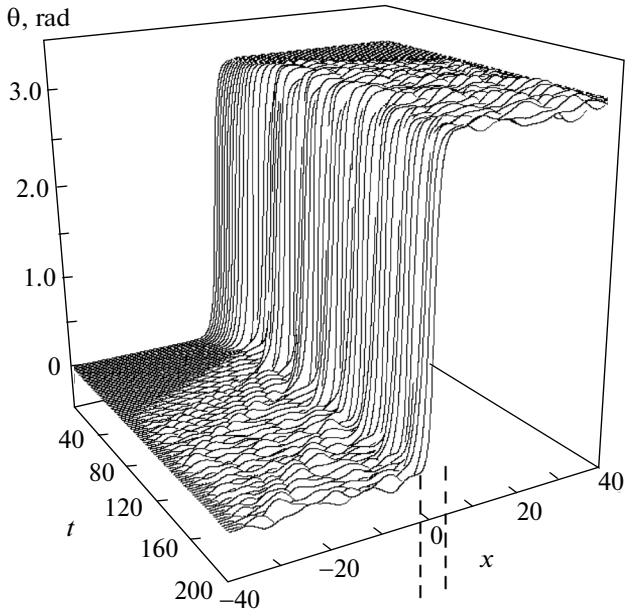

Fig. 2. Localization of the kink in the SMPP region (bounded by the dashed lines) for $\Delta K = 0$, $\Delta A = -0.5$, $W = 4$, $v = 0.1$, and $h = 0$.

a translation mode associated with oscillations of the kink's center of mass, we observe a fluctuation mode associated with variations in the kink width.

To verify the performance of the numerical scheme, we consider the analytical solution of the perturbed sine-Gordon equation (1) with the use of solution (2) with a time-dependent velocity $u(t)$:

$$\theta = 2\arctan\left(\exp\left(\pm\frac{x - X(t)}{\sqrt{1 - u^2(t)}}\right)\right), \tag{11}$$

$$X(t) = \int_0^t u(t_1)dt_1 + x_0(t). \tag{12}$$

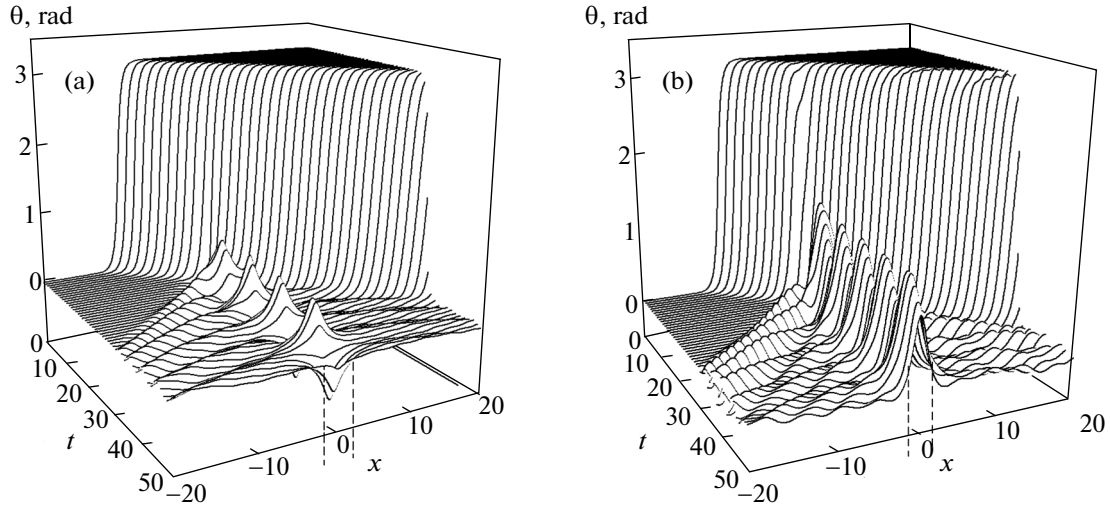

Fig. 3. Emergence and evolution of (a) a breather at rest for $A = 0.6$, $K = -1$, and $W = 2$; and (b) a soliton for $A = 0.6$, $K = -4$, and $W = 2$ in the SMPP region (bounded by the dashed lines).

Consider a kink moving at a sufficiently low velocity. Then the use of solution (12) is traditional and justified.

Perturbation theory (in the adiabatic approximation) [50] yields the following system of equations for $u(t)$ and $X(t)$:

$$\frac{du}{dt} = h(1-u^2)^{3/2} + \frac{1}{2}\left(\Delta A + \Delta K(1-u^2)\right)\sqrt{1-u^2}\int_{-\infty}^{\infty}\frac{1}{\cosh^2(\psi z\sqrt{1-u^2}+\psi X)}\frac{\sinh z}{\cosh^3 z}dz$$
$$+ \Delta A\psi(1-u^2)\int_{-\infty}^{\infty}\frac{\sinh(\psi z\sqrt{1-u^2}+\psi X)}{\cosh^3(\psi z\sqrt{1-u^2}+\psi X)}\frac{1}{\cosh^2 z}dz - \alpha u(1-u^2), \quad (13)$$

$$\frac{dX}{dt} = u + \frac{u}{2}\left(\Delta A + \Delta K(1-u^2)\right)\int_{-\infty}^{\infty}\frac{z}{\cosh^2(\psi z\sqrt{1-u^2}+\psi X)}\frac{\sinh z}{\cosh^3 z}dz$$
$$+ \Delta A\psi u\sqrt{1-u^2}\int_{-\infty}^{\infty}\frac{\sinh(\psi z\sqrt{1-u^2}+\psi X)}{\cosh^3(\psi z\sqrt{1-u^2}+\psi X)}\frac{z}{\cosh^2 z}dz - \alpha u(1-u^2), \quad (14)$$

where $\psi = 4/W$. System (13), (14) describes the time variations in $X(t)$ and $u(t)$. It is solved numerically by applying the fourth-order Runge–Kutta method with a step size of 0.01. Figure 1a shows that, for small SMPPs, the solution of system (13), (14) agrees well with the numerical solution of Eq. (1).

Inspection of the dynamics of a kink intersecting the SMPP region reveals that localized large-amplitude nonlinear waves of the soliton and breather types appear in this region. The numerical results show that the emergence and evolution of such waves follow various scenarios depending on K, A, and W. Although the time required for the kink to travel through the SMPP region is small (about ten time units), the process is accompanied by noticeable variations in the velocity and structure of the kink. All the results presented below were obtained for $\alpha = 0.01$ and $h = 0.016$. The choice of $h = 0.016$ is explained by the necessity to speed up the kink to the steady-state velocity required for intersecting the SMPP region with specified parameters K, A, and W.

Figure 3a displays a typical pattern of kink dynamics. After the kink goes away, a nonlinear wave appears in the SMPP region. Its amplitude is maximal at the center of the SMPP region and oscillates from $+\theta^*_{\max}$ to $-\theta^*_{\max}$. Note that the amplitude value depends strongly on the parameter K, A, and W. For the case presented in Fig. 3, Figure 4 (curve *1*) depicts $\theta^*(t)$ at the center of the SMPP region as a function of time. It can be seen that this is a periodic function with the oscillation frequency $\omega = 0.72$. The numer-

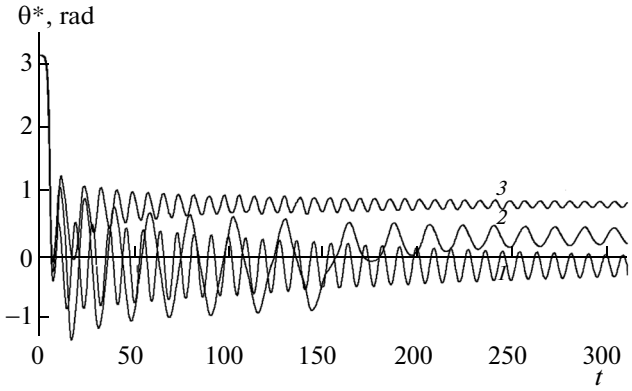

Fig. 4. The value θ^* at the center of the SMPP region as a function of time for $A = 0.6$, $W = 2$, and (*1*) $K = -1$, (*2*) $K = -2.3$, and (*3*) $K = -4$.

ically obtained function $\theta^*(t)$ coincides with formula (3) assuming that the amplitude is damped with time according to the formula

$$\theta = \theta^*_{\max} \exp(-\alpha(t - t_0)), \tag{15}$$

where $\theta^*_{\max} = 0.6$ and $x_0 = 0$. As a result, the localized nonlinear wave obtained in this case can be regarded as a breather at rest. Additionally, Fig. 3 shows that the breather is also damped due to radiated three-dimensional waves. The logarithmic decrement obtained from the approximation of the time dependence of θ^* is nearly equal to the prescribed value α; i.e., much of the breather energy dissipates through radiation.

When the parameters $(1 - A)$, $(1 - K)$, and W increase to a certain value, the evolution of the developing breather at rest changes. Curve (*2*) in Fig. 4 shows that, starting at $t = 160$, the oscillations of $\theta^*(t)$ continue only in the domain of positive θ. Note that the breather transforms into a soliton having a much higher oscillation frequency.

As $(1 - A)$, $(1 - K)$, and W increase further, an oscillating soliton appears in the SMPP region immediately after the kink has gone (Fig. 3b, curve *3* in Fig. 4). Whereas the breather amplitude vanishes with time, the soliton amplitude tends to a constant value $-\theta^*$. The numerically obtained dependence of θ^* on A, K, and W for SMPP of form (5) can be approximated by the formula

$$\cos\theta^* \approx 4 \cdot A^n / (|K| \cdot W^m), \tag{16}$$

where $n = 0.13$ and $m = 0.93$. Like the oscillation frequencies of the translational and fluctuation modes of the kink, the oscillation frequency ω_S of the soliton tends to unity with increasing $(1 - K)$ and W for all considered values of A. Additionally, ω_S decreases for $A > 1$ and increases for $A < 1$.

The ranges of A and K were determined for which breathers and solitons exist. Qualitatively, the dependence has the same form as in the case $A = 1$ (see [20]). As A increases, the curves shift toward larger values of $|K|$ and W.

Now, we consider the case of a nonzero external force and damping. Note also that in this case we obtain a double sine-Gordon equation, which has its own kink solution. The scheme for the numerical experiment is as follows: initially, a double sine-Gordon kink is specified at the center of an impurity that stabilizes its position. After the kink is numerically restructured due to the impurity, an external constant force is applied to it. As a result, the kink begins to move and escapes the SMPP region, while we observe the variations in the structure of nonlinear waves in this region.

Various SMPP parameters (5) and $\alpha = 0.01$ were used in the numerical computations. The value $h = 0.35$ was chosen so that, for smaller h, the external force was not sufficient for the kink to escape from the SMPP region, since it did not have enough energy to leave the potential well.

Examining the dynamics of the kink escaping the SMPP region, by analogy with the above case of nondissipative inertial motion, we found that a breather, a breather transforming into a soliton, and a soliton appear in this domain. The frequencies and oscillation amplitudes of breather- or soliton-type localized magnetic inhomogeneities were determined as follows: we found the point at which $d\theta/dx = 0$, and

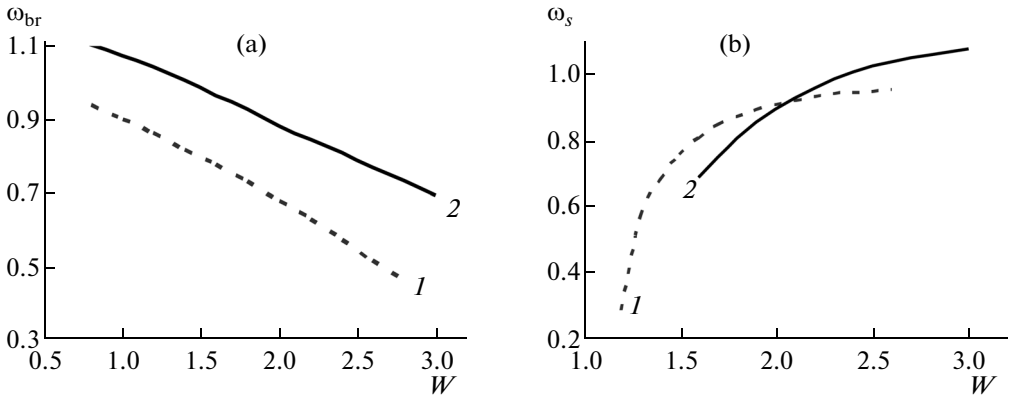

Fig. 5. Oscillation frequency as a function of W for (a) breather at $A = 1$ and $K = -4$ and for (b) soliton at $A = 1$ and $K = -1.2$ for (*1*) $h = 0.016$ and (*2*) $h = 0.35$.

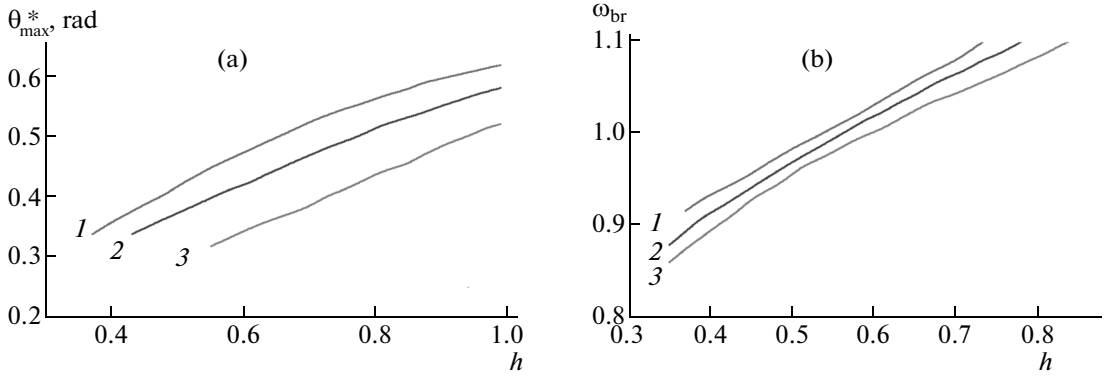

Fig. 6. (a) Maximum amplitude $\theta^*_{\max}$ and (b) the oscillation frequency ω_{br} of the breather as a function of h for $W = 2$, $K = -1.2$, and (*1*) $A = 1.4$, (*2*) $A = 1$, and (*3*) $A = 0.6$.

obtained the node index i_0 corresponding to this point. Under the conditions $\theta^k_{i_0} > \theta^{k+1}_{i_0}$ and $\theta^{k-1}_{i_0} > \theta^k_{i_0}$, we fixed the time $t_1 = t_k$ corresponding to the maximum value $\theta(x, t) = \theta_{\max}$. Next, under the conditions $\theta^k_{i_0} < \theta^{k+1}_{i_0}$ and $\theta^k_{i_0} < \theta^{k-1}_{i_0}$, we fixed the time $t_2 = t_k$ corresponding to the maximum value $\theta(x, t) = \theta_{\min}$. The difference $t_2 - t_1$ was equal to half an oscillation period. The period and the cyclic frequency were determined using the formulas $T = 2(t_2 - t_1)$ and $\omega = 2\pi/T$, while the oscillation amplitude was $(\theta_{\max} - \theta_{\min})/2$. The dependences of the oscillation amplitude and frequency on K, A, and W were found to be similar to the above case $h = 0$.

Figure 5 shows the oscillation frequencies of the (a) soliton and (b) breather as functions of W for two different external forces, namely, (*1*) $h = 0.016$ and (*2*) $h = 0.35$. For the breather (Fig. 5a), the curves are nearly parallel to each other with the higher one corresponding to the larger value of h. The difference between the frequencies for different h is at least 15%. In Fig. 5b (the soliton case), the curves intersect, which suggests that the external force has a large effect in this case and indicates the form of the dependence. The curve for $h = 0.35$ is higher only when W is greater than two. Note also that, as h increases, the soliton appears for larger K, A, and W. Figures 6 and 7 suggest that the dynamical parameters of localized nonlinear waves can be effectively controlled by varying the external force. For example, the breather oscillation frequency ω_{br} vs. h (Fig. 6b) is close to a linear function, while, the soliton oscillation frequency is $\omega_s(h) \sim \omega_0 - (ah)^b/\sqrt{1 + (ah)^{2b}}$, where a and b are constants and $a, b > 0$, ω_0 is the soliton oscillation frequency at $h = 0$ (Fig. 7b). The dependence of the breather oscillation amplitude θ^* on h (Fig. 6a)

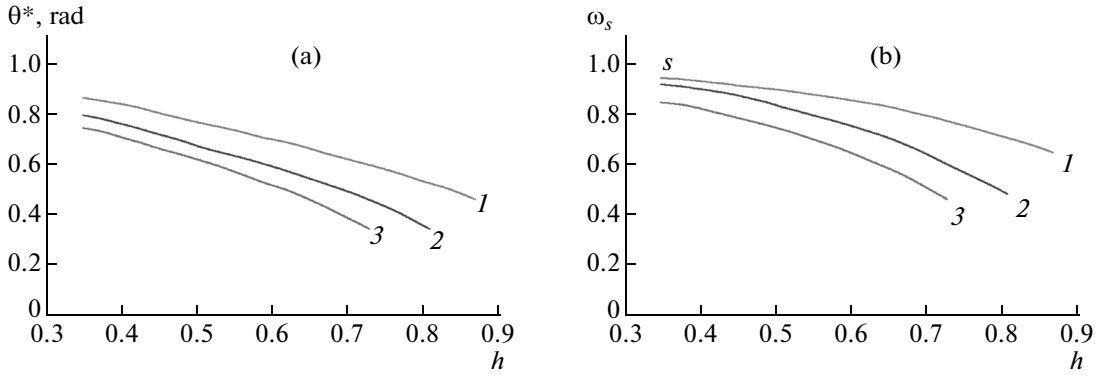

Fig. 7. (a) Maximum amplitude θ^* and (b) the oscillation frequency ω_S of the soliton as a function of h for $W = 2$, $K = -4$, and (*1*) $A = 1.4$, (*2*) $A = 1$, and (*3*) $A = 0.6$.

is similar to the frequency dependence and is close to a linear function. The dependence of the soliton oscillation amplitude on h is also similar to the frequency dependence (see Fig. 7a).

CONCLUSIONS

The dynamics of sine-Gordon kinks was studied in the presence of an external force, damping, and a spatially modulated periodic potential. The minimum velocity required for a kink to pass through the spatial modulation region was calculated. The cases in which the numerical results agree well with the analytical ones were indicated. The emergence, structure, and characteristics of large-amplitude localized nonlinear waves of the soliton and breather types were investigated by applying numerical methods. The influence of an external force on excited localized nonlinear waves was examined. The dependences of the oscillation frequencies and amplitudes on the parameters of the system were found.

REFERENCES

1. *Encyclopedia of Nonlinear Science*, Ed. by A. Scott (Routledge, New York, 2004).
2. M. A. Shamsutdinov, V. N. Nazarov, I. Yu. Lomakina, et al., *Ferro- and Antiferromagnetic Dynamics: Nonlinear Oscillations, Waves, and Solitons* (Nauka, Moscow, 2009) [in Russian].
3. O. M. Braun and Yu. S. Kivshar, *The Frenkel–Kontorova Model: Concepts, Methods, and Applications* (Springer, Berlin, 2004; Fizmatlit, Moscow, 2008).
4. T. Dauxois and M. Peyrard, *Physics of Solitons* (Cambridge Univ. Press, New York, 2010).
5. M. B. Fogel, S. E. Trullinger, A. R. Bishop, and J. A. Krumhandl, "Dynamics of sine-Gordon solitons in the presence of perturbations," Phys. Rev. B **15**, 1578–1592 (1977).
6. J. P. Currie, S. E. Trullinger, A. R. Bishop, and J. A. Krumhandl, "Numerical simulation of sine-Gordon soliton dynamics in the presence of perturbations," Phys. Rev. B **15** (12), 5567–5580 (1977).
7. R. H. Goodman, P. J. Holmes, and M. I. Weinstein, "Interaction of sine-Gordon kinks with defects: Phase space transport in a two-mode model," Physica D: Nonlinear Phenomena **161** (1), 21–44 (2002).
8. J. A. González, A. Bellorin, and L. E. Guerrero, "Internal modes of sine-Gordon solitons in the presence of spatiotemporal perturbations," Phys. Rev. E (Rapid Commun.) **65**, 065601 (2002).
9. S. Nazifkar and K. Javidan, "Collective coordinate analysis for double sine-Gordon model," Brazil. J. Phys. **40** (1), 102–107 (2010).
10. J. A. González, S. Cuenda, and A. Sánchez, "Kink dynamics in spatially inhomogeneous media: The role of internal modes," Phys. Rev. E **75**, 036611 (2007).
11. A. G. Bratsos, "The solution of the two-dimensional sine-Gordon equation using the method of lines," J. Comput. Appl. Math. **206** (1), 251–277 (2007).
12. A. L. Fabian, R. Kohl, and A. Biswas, "Perturbation of topological solitons due to sine-Gordon equation and its type," Commun. Nonlinear Sci. Numer. Simul. **14** (4), 1227–1244 (2009).

13. B. Batiha, M. S. M. Noorani, and I. Hashim, "Numerical solution of sine-Gordon equation by variational iteration method," Phys. Lett. A **370** (5), 437–440 (2007).
14. M. J. Ablowitz, B. M. Herbst, and C. M. Schober, "On the numerical solution of the sine-Gordon equation," J. Comput. Phys. **131** (2), 354–367 (1997).
15. D. I. Paul, "Soliton theory and the dynamics of a ferromagnetic domain wall," J. Phys. C: Solid State Phys. **12**, 585–593 (1979).
16. C. J. K. Knight, G. Derks, A. Doelman, and H. Susanto, "Stability of stationary fronts in a nonlinear wave equation with spatial inhomogeneity," J. Differ. Equations **254** (2), 408–468 (2013).
17. B. Piette, W. J. Zakrzewski, and J. Brand, "Scattering of topological solitons on holes and barriers," J. Phys. A: Math. General **38** (48), 10403–10412 (2005).
18. B. Piette and W. J. Zakrzewski, "Scattering of sine-Gordon kinks on potential wells," J. Physics A: Math. Theor. **40**, 5995–6010 (2007).
19. E. G. Ekomasov and A. M. Gumerov, "Simulation of the interaction of nonlinear waves in the sine-Gordon model for materials with defects," Perspektiv. Mater., No. 12, 104–108 (2011).
20. E. G. Ekomasov, Sh. A. Azamatov, and R. R. Murtazin, "Study of excitation and evolution of soliton- and breaser-type magnetic inhomogeneities in magnets with local anisotropy inhomogeneities," Fiz. Metallov Metalloved. **105** (4), 341–349 (2008).
21. E. G. Ekomasov, A. M. Gumerov, R. R. Murtazin, et al., "Excitation of high-amplitude localized nonlinear waves as a result of interaction of kink with attractive impurity in sine-Gordon equation," arXiv:1307.3470 [nlin.PS] (2013).
22. E. G. Ekomasov, A. M. Gumerov, and R. R. Murtazin, "Combined effect of impurities on the dynamics of kinks in the modified sine-Gordon equation," Komp'yut. Issled. Model. **5** (3), 403–412 (2013).
23. A. M. Gumerov, E. G. Ekomasov, F. K. Zakir'yanov, and R. V. Kudryavtsev, "Structure and properties of four-kink multisolitons of the sine-Gordon equation," Comput. Math. Math. Phys. **54** (3), 491–504 (2014).
24. E. G. Ekomasov, A. M. Gumerov, and I. I. Rakhmatullin, "Numerical simulation of pinning and nonlinear dynamics of domain walls in ferromagnets with defects," Vestn. Bashkir. Univ. **15** (3), 564–566 (2010).
25. S. W. Goatham, L. E. Mannering, R. Hann, and S. Krusch, "Dynamics of multi-kinks in the presence of wells and barriers," Acta Phys. Polonica B **42** (10), 2087–2106 (2011).
26. S. P. Popov, "Influence of dislocations on kink solutions of the double sine-Gordon equation," Comput. Math. Math. Phys. **53** (12), 1891–1899 (2013).
27. E. G. Ekomasov, R. R. Murtazin, O. B. Bogomazova, and A. R. Al'mukhametova, "Nonlinear dynamics of sine-Gordon kinks in the presence of localized spatial modulation of system's parameters," Vestn. Bashkir. Univ. **17** (2), 847–852 (2012).
28. E. G. Ekomasov, R. R. Murtazin, O. B. Bogomazova, and A. M. Gumerov, "One-dimensional dynamics of domain walls in two-layer ferromagnet structure with different parameters of magnetic anisotropy and exchange," J. Magn. Magn. Mater. **339**, 133 (2013).
29. A. Mohebbi and M. Dehghan, "High-order solution of one-dimensional sine-Gordon equation using compact finite difference and DIRKN methods," Math. Comput. Model. **51** (5–6), 537–549 (2010).
30. P. J. Van der Houwen, B. P. Sommeijer, and N. H. Cong, "Parallel diagonally implicit Runge–Kutta–Nyström Methods," Appl. Numer. Math. **9** (2), 111–131 (1992).
31. M. Dehghan and A. Shokri, "Numerical method for one-dimensional nonlinear sine-gordon equation using collocation and radial basis functions," Numer. Methods Partial Differ. Equations **24** (2), 687–698 (2008).
32. A. G. Bratsos and E. H. Twizell, "The solution of the sine-Gordon equation using the method of lines," Int. J. Comput. Math. **61** (3–4), 271–292 (1996).
33. Z. Soori and A. Aminataei, "The spectral method for solving sine-Gordon equation using a new orthogonal polynomial," Appl. Math. **2012**, Article ID 462731 (2012) doi:10.5402/2012/462731.
34. G. L. Alfimov, W. A. B. Evans, and L. Vázquez, "On radial sine-Gordon breathers," Nonlinearity **13**, 1657–1680 (2000).
35. S. P. Popov, "Application of the quasi-spectral Fourier method to soliton equations," Comput. Math. Math. Phys. **50** (12), 2064–2070 (2010).
36. Ma Li-Min and Wu Zong-Min, "A numerical method for one-dimensional nonlinear sine-Gordon equation using multiquadric quasi-interpolation," Chinese Phys. **18** (8), 3099.
37. A. G. Bratsos, "A numerical method for the one-dimensional sine-Gordon equation," Numer. Methods Partial Differ. Equations **24** (3), 833–844 (2008).
38. A. Q. M. Khaliq, B. Abukhodair, Q. Sheng, and M. S. Ismail, "A predictor-corrector scheme for the sine-Gordon equation," Numer. Methods Partial Differ. Equations **16** (2), 133–146 (2000).

39. A. Akgul and M. Inc, "Numerical solution of one-dimensional sine-Gordon equation using reproducing kernel Hilbert space method," arXiv:1304.0534 [math.NA] (2013), http://arxiv.org/abs/1304.0534v1.
40. A. A. Samarskii, *The Theory of Difference Schemes* (Nauka, Moscow, 1989; Marcel Dekker, New York, 2001).
41. N. S. Bakhvalov, N. P. Zhidkov, and G. M. Kobel'kov, *Numerical Methods* (Nauka, Moscow, 1987) [in Russian].
42. S. E. Koonin, *Computational Physics: FORTRAN Version* (Addison-Wesley, Redwood City, Ca, 1990; Mir, Moscow, 1992).
43. L. A. Ferreira, B. Piette, and W. J. Zakrzewski, "Wobbles and other kink-breather solutions of sine-Gordon model," Phys. Rev. E **77**, 036616 (2008).
44. G. Kalberman, "The sine-Gordon wobble," J. Phys. A: Math. Gen. **37**, 11603–11612 (2004).
45. T. Sh. Kal'menov and D. Suragan, "Transfer of Sommerfeld radiation conditions to the boundary of a bounded domain," Vychisl. Mat. Mat. Fiz. **52** (6), 1063–1068 (2012).
46. W. F. Chang and G. A. McMechan, "Absorbing boundary conditions for 3-D acoustic and elastic finite-difference calculations," Bull. Seismol. Soc. Am. **79** (1), 211–218 (1989).
47. B. Engquist and A. Majda, "Radiation boundary conditions for acoustic and elastic wave calculations," Commun. Pure Appl. Math. **32** (3), 313–357 (1979).
48. A. A. Konstantinov, V. P. Maslov, and A. M. Chebotarev, "Shift of the boundary conditions for partial differential equations," USSR Comput. Math. Math. Phys. **28** (6), 111–121 (1988).
49. R. L. Higdon, "Numerical absorbing boundary conditions for the wave equation," Math. Comput. **49** (179), 65–90 (1987).
50. E. S. Shikhovtseva and V. N. Nazarov, "Effect of the nonlinear longitudinal compression on the conformational dynamics of the bistable quasi-one-dimensional macromolecules," JETP Lett. **86** (8), 497–501 (2007).

Translated by I. Ruzanova